

VIP Photocatalytic H₂ Production Very Important Paper
How to cite: *Angew. Chem. Int. Ed.* **2022**, *61*, e202114071

International Edition: doi.org/10.1002/anie.202114071

German Edition: doi.org/10.1002/ange.202114071

Enhancing Photocatalytic Hydrogen Production via the Construction of Robust Multivariate Ti-MOF/COF Composites

Cheng-Xia Chen, Yang-Yang Xiong, Xin Zhong, Pui Ching Lan, Zhang-Wen Wei, Hongjun Pan, Pei-Yang Su, Yujie Song, Yi-Fan Chen,* Ayman Nafady, Sirajuddin, and Shengqian Ma*

Abstract: Titanium metal–organic frameworks (Ti-MOFs), as an appealing type of artificial photocatalyst, have shown great potential in the field of solar energy conversion due to their well-studied photoredox activity (similar to TiO₂) and good optical responsiveness of linkers, which serve as the antenna to absorb visible-light. Although much effort has been dedicated to developing Ti-MOFs with high photocatalytic activity, their solar energy conversion performances are still poor. Herein, we have implemented a covalent-integration strategy to construct a series of multivariate Ti-MOF/COF hybrid materials PdTCPP-CPCN-415(NH₂)/TpPa (composites 1, 2, and 3), featuring excellent visible-light utilization, a suitable band gap, and high surface area for photocatalytic H₂ production. Notably, the resulting composites demonstrated remarkably enhanced visible-light-driven photocatalytic H₂ evolution performance, especially for the composite 2 with a maximum H₂ evolution rate of 13.98 mmol g⁻¹ h⁻¹ (turnover frequency (TOF) = 227 h⁻¹), which is much higher than that of PdTCPP-CPCN-415(NH₂) (0.21 mmol g⁻¹ h⁻¹) and TpPa (6.51 mmol g⁻¹ h⁻¹). Our work thereby suggests a new approach to highly efficient photocatalysts for H₂ evolution and beyond.

Introduction

Converting solar energy to sustainable and renewable energy sources is one of the most promising solutions to address the global energy crisis and environmental pollution issue.^[1] Among these, photocatalytic hydrogen production from water splitting has become a targeted goal of human society to gain clean energy.^[2] Although a great deal of effort has been devoted to developing photocatalysts, including molecular photocatalysts,^[3] organic and inorganic semiconductors,^[4] and their composites,^[5] for effective hydrogen

evolution, it remains challenging to achieve efficient visible-light conversion, rapid separation of photogenerated electrons (e) from holes (h), and sustainable recyclability. Because of its high effectiveness, stability, abundance, and low toxicity, titania (TiO₂) has been widely used for water splitting reaction to generate hydrogen.^[1d,6] However, the poor visible-light responsiveness and the detrimental photo-generated e-h recombination of TiO₂ severely impedes its practical application due to its intrinsically wide band gap (≈3.2 eV) and the easy aggregation during its nano-sized preparation process.^[7] Given that visible-light accounts for about 42–43 % of solar energy, extending the light absorption to the visible-light region will significantly improve solar energy capture capacity thereby affording high photocatalytic activity.^[8] Moreover, constructing porous semiconductors based on TiO₂ can promote the photogenerated e-h separation owing to the high surface area and porosity.^[1c,7,9]

As a class of porous semiconductors, titanium metal–organic frameworks (Ti-MOFs), constructed from the coordination of Ti-oxo clusters and organic ligand, have shown great potential in photocatalysis benefiting from their high surface area, excellent chemical stability, and tunable functionalities.^[10] The Ti-oxo clusters acting as the analogs of TiO₂ can impart Ti-MOFs with photocatalytic activity;^[11] the highly crystalline nature can make the photosensitizers and catalytic sites configured in the microcrystalline lattice, which effectively suppresses the recombination of photogenerated e-h; additionally, the outstanding surface area and porosity facilitate the substrate/product transport and access to the active sites, endowing Ti-MOFs with excellent photocatalytic activity and good recyclability. More importantly, the optical responsiveness and band gaps can be finely tuned by judiciously changing the photoactivity of organic ligands.^[10b,f,12] However, the photocatalytic hydrogen evolution

[*] X. Zhong, Y. Song, Dr. Y.-F. Chen
 School of Chemical Engineering and Technology, Hainan University
 Haikou 570228 (China)
 E-mail: cheniyifan@hainanu.edu.cn



Dr. C.-X. Chen, P. C. Lan, Dr. H. Pan, Prof. S. Ma
 Department of Chemistry, University of North Texas
 1508 W Mulberry St, Denton, TX 76201 (USA)
 E-mail: shengqian.ma@unt.edu

Y.-Y. Xiong, Dr. Z.-W. Wei
 Lehn Institute of Functional Materials, School of Chemistry
 Sun Yat-sen University
 Guangzhou 510275 (China)

Dr. P.-Y. Su
 Institute of Environmental Research at Greater Bay Area
 Guangzhou University
 Guangzhou 510006 (China)

Prof. A. Nafady
 Department of Chemistry, College of Science, King Saud University
 Riyadh 11451 (Saudi Arabia)

Dr. Sirajuddin
 HEJ Research Institute of Chemistry, International Centre for
 Chemical and Biological Sciences, University of Karachi
 75270 Karachi (Pakistan)

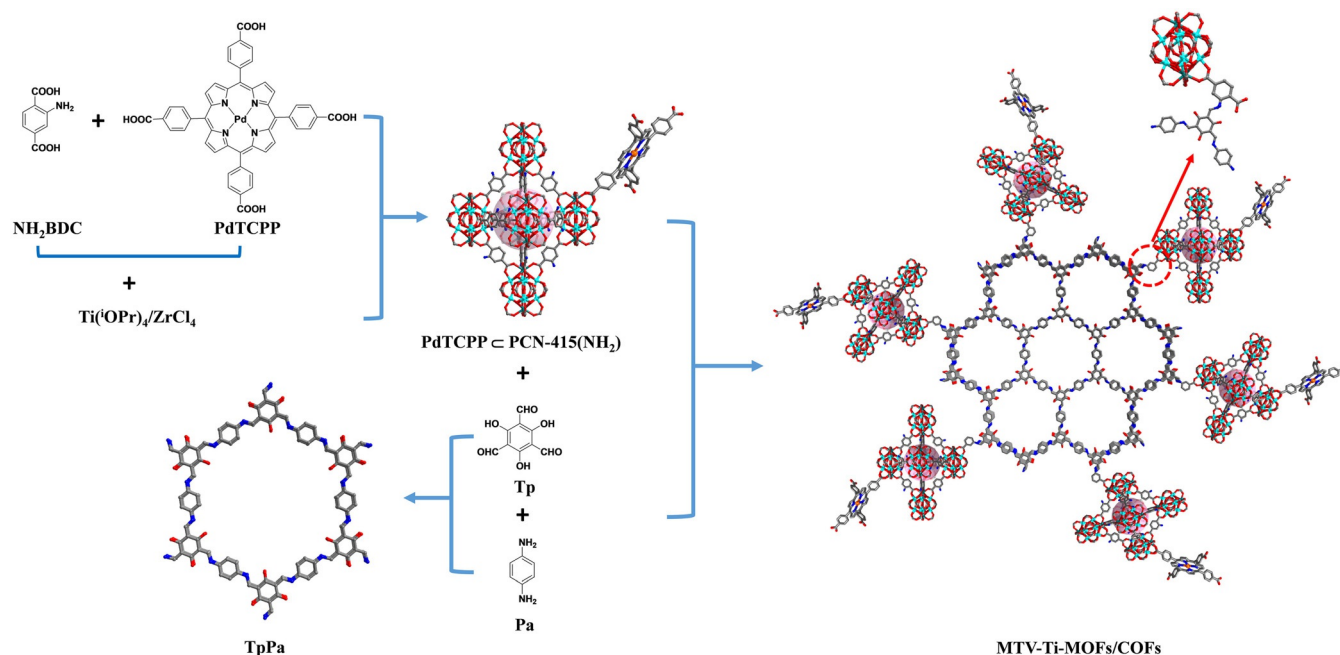
 Supporting information and the ORCID identification number(s) for the author(s) of this article can be found under:
 <https://doi.org/10.1002/anie.202114071>.

performance of Ti-MOFs currently is still poor as a result of the low visible-light utilization.

One key for enhancing the photocatalytic activities of Ti-MOFs is to expand the visible-light response range, which can be achieved through the construction of multi-functionalization via introducing appropriate functional groups like metalloporphyrin^[13] or the hybridization with other functional materials including covalent organic frameworks (COFs),^[14] metal nanoparticles,^[15] and organic dyes.^[16] These approaches can bestow the resulting composites with greater photocatalytic traits than their parent Ti-MOFs from the synergistic effects. As a type of well-known artificial light-harvesting molecules, metalloporphyrins, such as Pd-, Pt-, and Rh-porphyrins,^[17] have been extensively explored to mimic the natural photocatalysis due to the following merits: (i) the favorable energy position of porphyrins can facilitate the production of photoexcited carriers under visible-light irradiation; (ii) the conjugate macrocycle structure with multiple-anchors in porphyrins can promote the charge separation and the electron mobility during photocatalytic process; and (iii) porphyrin rings consisted of four tetrapyrrole moieties can coordinate and stabilize different metal ions to work as the light-harvesting center or active catalysis center. Therefore, introducing metalloporphyrin ligands into MOFs to construct multivariate Ti-MOFs (MTV-Ti-MOFs) via coordination bond will give rise to effective photocatalytic conversion performance. More recently, COFs, especially imine-based COFs, acting as a new class of crystalline porous materials constructed by covalent bonds, have exhibited notable potential in photocatalysis due to excellent optical response, good crystallinity, high porosity, and tunable functionalization.^[18] The well-stacked π - π arrays can result in high photoconductivity or charge mobility, thereby meditating the electronic interaction for enhanced charge transfer

capability. Additionally, the imine-based COFs usually include homogeneously distributed heteroatoms (N) which can render them the ability to anchor and disperse metal nanoparticles. Taken altogether, we anticipate that combining the metalloporphyrin functional MTV-Ti-MOFs with imine-based COFs will not only inherit the characteristics of parent species but also afford superior photocatalysis that individual pristine species can hardly achieve.

Herein, we report a new type of MTV-Ti-MOF/COF hybrid photocatalysts through implementing a covalent-integration strategy for visible-light-driven photocatalytic H₂ production. Tetratopic Pd-porphyrin ligand was chosen to incorporate into PCN-415(NH₂)^[10b] through in situ one-pot synthesis based on coordination bonding, giving rise to a MTV-Ti-MOF, PdTCPP@PCN-415(NH₂), which features the integration of desired multi-functionalities and high chemical stability (Scheme 1).^[19] The 2D imine-based COFs, TpPa, was selected to construct the hybrid materials due to its matching band gaps and effective visible-light adsorption performance.^[18] A series of PdTCPP@PCN-415(NH₂)/TpPa composites with different amounts of MOFs, denoted as 1, 2, and 3, were synthesized by covalently connecting -NH₂ of MTV-Ti-MOFs with the -CHO of COFs during the synthetic process of TpPa (Scheme 1). The resulting 1, 2, and 3 present efficient visible-light-driven photocatalytic H₂ evolution performances attributed to the excellent optical response, suitable band gap, and high surface area. Remarkably, composite 2 represents the best photocatalytic activity with a maximum H₂ evolution rate of 13.98 mmol g⁻¹ h⁻¹ (TOF = 227 h⁻¹), which is much higher than the prototypical counterparts, PdTCPP@PCN-415(NH₂) (0.21 mmol g⁻¹ h⁻¹) and TpPa (6.51 mmol g⁻¹ h⁻¹), and is one of the best photocatalysts for H₂ evolution among MOFs- and COFs-based photocatalysts (Supporting Information, Table S3) reported thus



Scheme 1. The schematic synthesis of MTV-Ti-MOF/COF.

far.^[12b,14b,17b,18c,20] Moreover, the photocatalytic mechanism has been well elucidated by the steady-state photoluminescence spectra, apparent quantum efficiency experiments, and molecular simulation.

Results and Discussion

PdTCPP@PCN-415(NH₂) was obtained through solvothermal reaction of NH₂BDC, PdTCPP with Ti(OPr)₄/ZrCl₄ in *N,N*-dimethylformamide (DMF) at 135 °C (Scheme 1). The ratio of NH₂BDC and PdTCPP is 16.3:1 as determined through ¹H NMR of digested PdTCPP@PCN-415(NH₂) sample (Supporting Information, Figure S2). TpPa was chosen to construct the hybrid materials given the dynamic reversible feature of imine-bond and enol-ketone interconversion, which can transform into ultra-stable keto-amine moieties (irreversible) (Scheme 1). Both the synthesized PdTCPP@PCN-415(NH₂) and TpPa powders present highly crystalline powder X-ray diffraction (PXRD) patterns, which are consistent with the simulated PXRD (Figure S3). Three MTV-Ti-MOF/COF hybrid materials, denoted as 1, 2, and 3, were produced by doping different amount of PdTCPP@PCN-415(NH₂) into the reaction system of TpPa at 120 °C for 5 days (Scheme 1). The PXRD patterns of all the three composites match very well with simulated patterns of PdTCPP@PCN-415(NH₂) and TpPa, confirming the formation of TpPa and the structural preservation of PdTCPP@PCN-415(NH₂) after the assembly process (Figure S3). The ¹³C CP/MAS NMR spectra of composite 2 is consistent with that of PdTCPP@PCN-415(NH₂) and TpPa, further proving the successful formation of hybrid materials (Figure S4). The FT-IR spectra agree well with PdTCPP@PCN-415(NH₂) and TpPa (Figure S5). Notably, the peak at $\approx 1620\text{ cm}^{-1}$ corresponds to the typical stretching band of -C=N, suggesting the formation of imine-based bond between PdTCPP@PCN-415(NH₂) and TpPa (Figure S6). In addition, the X-ray photoelectron spectroscopy (XPS) analysis for composite 2 was performed to further confirm the existence of -C=N bond with the binding energy at 288.3 eV (Figure S7).

Thermogravimetric analyses (TGA) were carried out to evaluate their thermostability, revealing that all three hybrid materials can be stable up to 350 °C (Figure S8). N₂ (77 K) sorption isotherms were performed to assess their permanent porosity (Figure 1 a; Figure S9, Table S1). The Brunauer-Emmett-Teller (BET) surface area (S_{BET}) of TpPa is $996\text{ m}^2\text{ g}^{-1}$, whereas the value is $487\text{ m}^2\text{ g}^{-1}$ for PdTCPP@PCN-415(NH₂). With the increasing amount of PdTCPP@PCN-415(NH₂), the S_{BET} of three composites gradually decrease, with the values of 680 (composite 1), 653 (composite 2), and 594 (composite 3) $\text{m}^2\text{ g}^{-1}$, respectively, which are much higher than PdTCPP@PCN-415(NH₂). The total pore volumes of all the three synthesized composites are 0.39 (composite 1), 0.39 (composite 2) and 0.33 (composites 3) $\text{cm}^3\text{ g}^{-1}$, respectively. The pore size distribution of composites 1, 2, and 3 based on the density functional theory (DFT) are comparable with the reported values (Figure S15). The scanning electron microscope (SEM) analyses indicate that

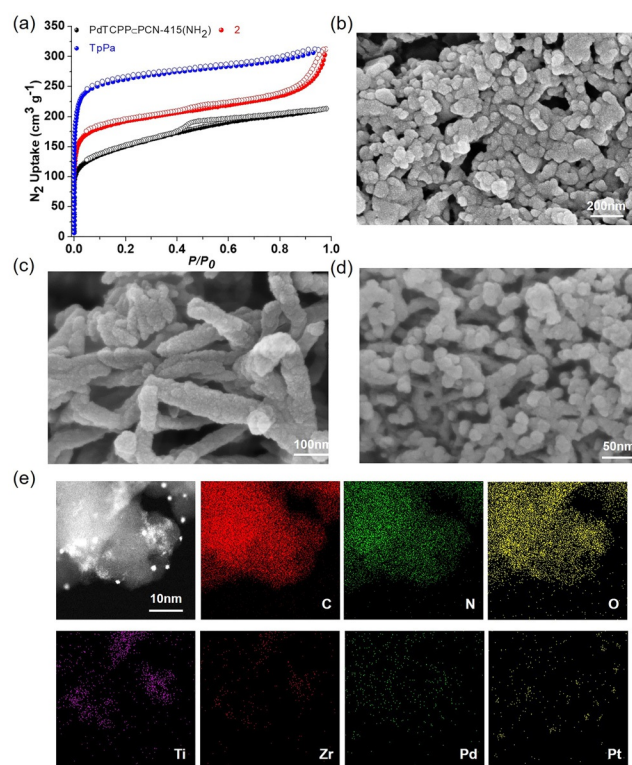


Figure 1. a) The N₂ adsorption isotherms of PdTCPP@PCN-415(NH₂), TpPa, and composite 2. b) SEM images of PdTCPP@PCN-415(NH₂), c) TpPa, and d) composite 2. e) HTEM images and the corresponding elemental mappings of C, N, O, Ti, Zr, Pd, and Pt for Pt@2.

the morphology of as-synthesized PdTCPP@PCN-415(NH₂) and TpPa samples are uniform (Figure 1 b,c). The different morphologies of PdTCPP@PCN-415(NH₂) and TpPa make them easily to distinguish, manifesting that PdTCPP@PCN-415(NH₂) nanoparticles can be uniformly attached on the surface of TpPa samples (Figure 1 d). The aberration-corrected high-angle annular dark-field scanning transmission electron microscopy (HAADF-STEM) images were performed to unveil the uniform stick-like morphology of composites (Figure S16). Furthermore, the images of element mapping were carried out to confirm that C, N, O, Ti, Zr, Pd are evenly distributed throughout the entire framework (Figure 1 e).

The UV-vis diffuse reflectance spectra (DRS) were measured to manifest that PdTCPP@PCN-415(NH₂) exhibits broadly intense optical absorbance below 850 nm, covering the whole UV/vis region even near infrared, whereas TpPa presents intense absorbance below 640 nm (Figure 2 a; Figure S19). The hybrid materials, 1, 2, and 3, not only inherit the optical nature of TpPa, but also display more intense optical absorbance from 640 to 850 nm due to the introduction of PdTCPP@PCN-415(NH₂) (Figure S19). The optical band gaps of PdTCPP@PCN-415(NH₂) and TpPa were estimated to be 1.75 and 2.05 eV, respectively, on the basis of the UV-vis DRS, suggesting excellent adsorption in visible-light region (Figure S20). Notably, PdTCPP@PCN-415(NH₂) presents a significantly decreased optical band gap compared with PCN-415(NH₂) (1.99 eV)^[10b] resulted from the introduction of PdTCPP ligand with excellent visible-light adsorption.

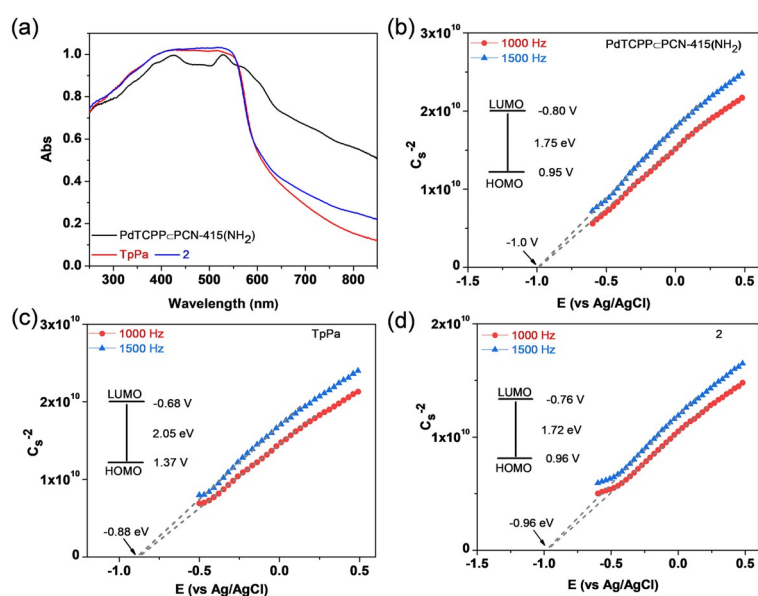


Figure 2. a) The solid diffuse reflectance spectra of PdTCPP-PCN-415(NH₂), TpPa, and composite 2. b–d) The Mott-Schottky plots, HOMO (inset), LUMO (inset), and band gaps (inset) of PdTCPP-PCN-415(NH₂), TpPa and composite 2.

Similarly, the optical band gap of composite 2 was calculated to be 1.72 eV (Figure S20). The Mott-Schottky (M-S) measurements were performed to determine the flat band positions of PdTCPP-PCN-415(NH₂), TpPa, and composite 2, with the values of -1.00 , -0.88 , and -0.96 eV vs. Ag/AgCl, respectively (Figure 2). Strikingly, the slope of M-S plot for composite 2 is lower than PCN-415(NH₂),^[10b] indicating the electron density has increased obviously due to the introduction of PdTCPP ligand and the covalent integration between the MTV-Ti-MOFs and COFs. In addition, the positive slope of M-S plots indicates that both the MTV-MOFs and COFs are n-type semiconductors. Given that the bottom of lowest unoccupied molecular orbital (LUMO) in typical n-type semiconductors is equal to the flat-band potential,^[21] the LUMO position of PdTCPP-PCN-415(NH₂) and TpPa are estimated to be approximately -0.80 and -0.68 eV (vs. NHE), showing ample potential for photocatalytic H₂ production. Thereby, the highest occupied molecular orbital (HOMO) of PdTCPP-PCN-415(NH₂) and TpPa can be calculated to be 0.95 eV and 1.37 eV (vs. NHE), respectively. Owing to the hybrid feature of composite 2, the LUMO position is between PdTCPP-PCN-415(NH₂) and TpPa, with the value of around -0.76 eV. Combined with its band gap, the HOMO position of composite 2 is 0.96 eV (vs. NHE), confirming its type II heterojunction characteristic.^[22]

Prompted by the high stability, good porosity, excellent optical response, and photoactive metal clusters, photocatalytic H₂ production experiments were conducted under visible-light irradiation using a 300 W Xe lamp equipped with a 400 nm cut off filter. In general, 10 mg of the catalyst was dispersed in PBS buffer solution (50 mL of 0.1 M solution at PH = 7) with 100 mg

ascorbic acid (SA) as a sacrificial reagent, and potassium tetrachloroplatinate as precursor for in situ formation of platinum nanoparticles (Pt NPs) by photo-deposition as the cocatalyst. HAADF-STEM spectra show that the Pt NPs acted as bright spots uniformly disperse onto the composite 2 marked with red circles, which were further identified via HTEM images (Figures S16 and S18). The HTEM images of composite Pt@2 shows that the d-spacing between two adjacent lattice planes is about 0.23 nm, in agreement with the spacing of the Pt (111) plane (Figure S18). The images of elemental mapping confirm the homogeneous distribution nature of C, N, O, Ti, Zr, Pd and Pt throughout the whole structure (Figure 1e; Figure S17). Initially, the comparative experiments with different contents of Pt confirm that 1.2 wt % Pt loading is the best content for photocatalytic H₂ production (Figure S22). On the basis of the optimal catalytic condition, TpPa presents a H₂ evolution rate of 6.51 mmol g⁻¹ h⁻¹ after visible-light irradiation for 5 h, whereas PdTCPP-PCN-415(NH₂) displays considerably slow H₂ evolution rate (0.21 mmol g⁻¹ h⁻¹, Figure 3a). Significantly, the integrated hybrid composites show obvious enhanced H₂ evolution rate, with the maximum of 13.98 mmol g⁻¹ h⁻¹ for composite 2, which is more than twice of the pristine TpPa, and one of the best photocatalysts among MOFs- and COFs-based catalysts reported in literature (Figure 3a; Table S3).^[12b,14b,17b,18c,20] Notably, the H₂ evolution rate for composite 2 is 27.67 mmol g⁻¹ h⁻¹ after visible-light irradiation for 1 h, and gradually decreased to 19.37 mmol g⁻¹ h⁻¹ after 3 h, and finally decreased to 13.98 mmol g⁻¹ h⁻¹ after 5 h. Based on the loaded amount of Pt, the total turnover number (TON) for composite 2 are calculated to be ≈ 945 and ≈ 1136 after 3 and 5 h irradiation, corresponding to TOF values of ≈ 315 and ≈ 227 h⁻¹, respectively. Moreover, the recycle H₂ evolution experiment for composite 2 was conducted for over 120 h to evaluate its photocatalytic durability, unveiling its excellent photocatalytic stability in reused 24 consecutive cycles (Figure 3b). The TON for composite 2 is calculated to be 24508 after 120 h visible-light irradiation, corresponding to TOF values of ≈ 204 h⁻¹, respectively.

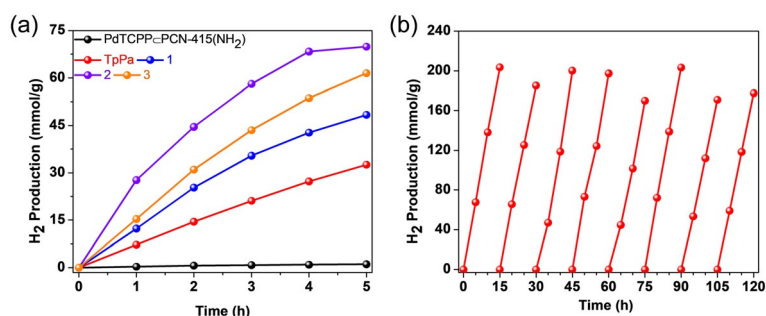


Figure 3. a) The photocatalytic H₂ evolution activities of PdTCPP-PCN-415(NH₂), TpPa, and the composites loaded with 1.2 wt % Pt. b) The photocatalytic H₂ evolution recyclability of composite 2.

To probe the photocatalytic reaction mechanism, the steady-state photoluminescence (PL) spectra of PdTCPP-PCN-415(NH₂), TpPa, and composite 2 were measured to evaluate their charge-separation efficiency (Figure 4a). TpPa displays an intensive emission with the maximum at 606 nm upon excitation ($\lambda_{\text{ex}} = 450$ nm), while PdTCPP-PCN-415(NH₂) exhibits a decreased emission intensity (maximum at 595 nm) due to the excellent visible-light adsorption of PdTCPP linkers. Remarkably, the covalently connecting hybrid material, composite 2, presents a significantly reduced PL intensity, suggesting the enhanced e-h separation efficiency. Moreover, the apparent quantum efficiency (AQY) of composites 2 were measured at 405, 450, and 515 nm using monochromatic LED light to examine their visible-light adsorption performance (Figure 4b; Table S2). For composite 2, the AQY were 2.9% at 405 nm, 5.7% at 450 nm, and 5.9% at 515 nm, respectively, clearly manifesting that the light conversion efficiency is highly dependent on the light-response range. In order to gain further insight into the photocatalytic activity, the density functional theory (DFT) calculations were performed to investigate the electronic structure of PdTCPP-PCN-415(NH₂) and TpPa. For PdTCPP-PCN-415(NH₂), the HOMO is mostly the C and N 2p orbitals originated from NH₂BDC, whereas the LUMO is mainly dominated by the d orbitals of Ti and Zr (Figure 4c,d). Thus, the electrons can transfer from the HOMO at NH₂BDC to the LUMO at Ti and Zr via the excitation of PdTCPP-PCN-415(NH₂) under visible-light irradiation, demonstrating a ligand-to-metal charge transfer (LMCT) process.^[10b] For TpPa, the HOMO is mainly the N and O 2p orbitals, while the LUMO is mostly dominated by the C 2p orbitals arising from the aromatic nucleus and -C-N bond (Figure S27).^[14b] Additionally, the calculated gaps of PdTCPP-PCN-415(NH₂) and TpPa are 1.23 and 1.72 eV. Taking into account the above experimental and theoretical

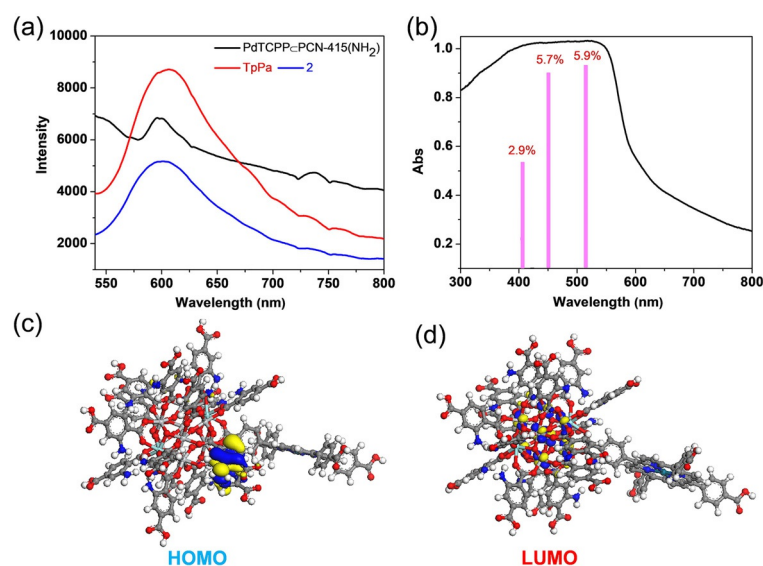


Figure 4. a) The photoluminescence spectra with the excitation wavelength of 450 nm. b) The apparent quantum yields of composite Pt@2 under the conditions of maximum photocatalytic H₂ evolution rate at $\lambda = 405, 450,$ and 515 nm. c,d) The molecular orbital diagrams of PdTCPP-PCN-415(NH₂).

results, the photocatalytic H₂ evolution mechanism is proposed in Figure 5. In composite 2, PdTCPP-PCN-415(NH₂) present excellent visible-light adsorption capacity, which can serve as an antenna to absorb light, transferring the photo-excited electrons to [Ti₈Zr₂O₁₂(COO)₁₆] clusters via LMCT. Then the photogenerated electrons on the clusters were

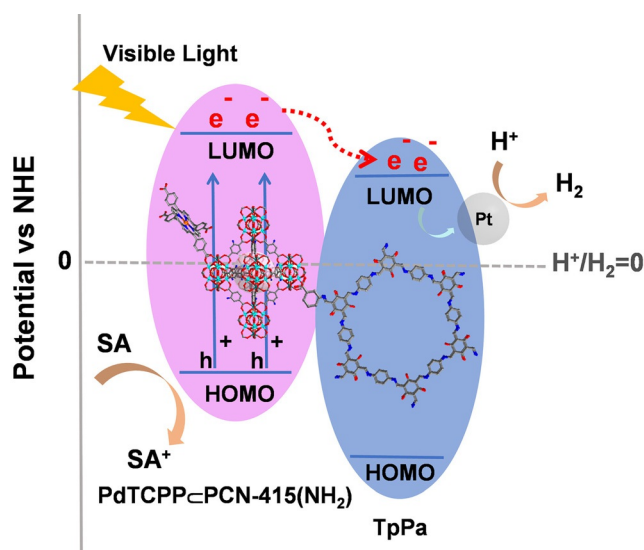


Figure 5. The photocatalytic H₂ evolution mechanism of composite 2.

further transferred to the LUMO of TpPa through the covalently connecting junction between PdTCPP-PCN-415(NH₂) and TpPa, guaranteeing the effective separation of photogenerated electrons and holes. Finally, the successfully photogenerated electrons in the LUMO of TpPa were transferred to the Pt NPs surface resulting in the H⁺ reduction process, whereas the photogenerated holes in the HOMO of PdTCPP-PCN-415(NH₂) were captured by the electron sacrificing agent SA, realizing the catalytic cycle.

Conclusion

In summary, a series of covalently connected MTV-Ti-MOF/COF hybrid materials have been successfully synthesized, featuring excellent visible-light responses, well-matched band gaps, and effective e-h separation for photocatalytic H₂ production. Results showed that the hybrid material 2, presented an excellent photocatalytic H₂ evolution performance with a TON value of 24 508 after irradiation for 120 h (TOF = 204 h⁻¹), which is much higher than the prototypical PdTCPP-PCN-415(NH₂) and TpPa counterparts, confirming the effectiveness of covalently linking the two distinct species. Additionally, experiments and theoretical calculations suggested that the excellent visible-light utilization and well-matched band gaps of PdTCPP-PCN-415(NH₂) and TpPa resulted in the superb photo-

catalytic H₂ evolution performance of the covalently integrated materials. This work contributes a novel covalent-integration strategy to construct MTV-Ti-MOF/COF hybrid materials for effective photocatalytic H₂ production, thus promoting the design of other MTV-MOF/COF hybrid materials for applications in photocatalysis and beyond.

Acknowledgements

This work was supported by the Robert A. Welch Foundation (B-0027) (S.M.). Partial support from the US National Science Foundation (ECCS- 2029800) (S.M.), NSFC (22001271, 21806027), Chinese Postdoctoral Science Found (2017M622866), the International Postdoctoral Exchange Fellowship Program (20180055), FRF for the Central Universities (20lgy79), and Researchers Supporting Project number (RSP-2021/79) at King Saud University, Riyadh, Saudi Arabia (A.N.) are also acknowledged.

Conflict of Interest

The authors declare no conflict of interest.

Keywords: covalent connecting junctions · covalent organic frameworks · hybrid materials · metal-organic frameworks · multivariate Ti-MOFs

- [1] a) T. Hisatomi, K. Domen, *Nat. Catal.* **2019**, *2*, 387–399; b) N. S. Lewis, D. G. Nocera, *Proc. Natl. Acad. Sci. USA* **2006**, *103*, 15729–15735; c) W. Li, A. Elzatahry, D. Aldhayan, D. Zhao, *Chem. Soc. Rev.* **2018**, *47*, 8203–8237; d) W. Zhang, H. He, H. Li, L. Duan, L. Zu, Y. Zhai, W. Li, L. Wang, H. Fu, D. Zhao, *Adv. Energy Mater.* **2021**, *11*, 2003303.
- [2] a) Y.-J. Yuan, Z.-T. Yu, D.-Q. Chen, Z.-G. Zou, *Chem. Soc. Rev.* **2017**, *46*, 603–631; b) J. Kou, C. Lu, J. Wang, Y. Chen, Z. Xu, R. S. Varma, *Chem. Rev.* **2017**, *117*, 1445–1514.
- [3] a) A. J. Esswein, D. G. Nocera, *Chem. Rev.* **2007**, *107*, 4022–4047; b) A. F. Heyduk, D. G. Nocera, *Science* **2001**, *293*, 1639–1641.
- [4] a) H. Tong, S. Ouyang, Y. Bi, N. Umezawa, M. Oshikiri, J. Ye, *Adv. Mater.* **2012**, *24*, 229–251; b) C. Xu, W. Yang, Q. Guo, D. Dai, M. Chen, X. Yang, *J. Am. Chem. Soc.* **2013**, *135*, 10206–10209; c) V. S. Vyas, V. W.-h. Lau, B. V. Lotsch, *Chem. Mater.* **2016**, *28*, 5191–5204; d) X. Ke, K. Dai, G. Zhu, J. Zhang, C. Liang, *Appl. Surf. Sci.* **2019**, *481*, 669–677.
- [5] a) Z. Li, J.-D. Xiao, H.-L. Jiang, *ACS Catal.* **2016**, *6*, 5359–5365; b) M. Wang, K. Han, S. Zhang, L. Sun, *Coord. Chem. Rev.* **2015**, *287*, 1–14.
- [6] a) T. Butburee, Y. Bai, H. Wang, H. Chen, Z. Wang, G. Liu, J. Zou, P. Khemthong, G. Q. M. Lu, L. Wang, *Adv. Mater.* **2018**, *30*, 1705666; b) Y. Ma, X. Wang, Y. Jia, X. Chen, H. Han, C. Li, *Chem. Rev.* **2014**, *114*, 9987–10043; c) M. Ge, C. Cao, J. Huang, S. Li, Z. Chen, K.-Q. Zhang, S. S. Al-Deyab, Y. Lai, *J. Mater. Chem. A* **2016**, *4*, 6772–6801; d) J. Tian, Z. Zhao, A. Kumar, R. I. Boughton, H. Liu, *Chem. Soc. Rev.* **2014**, *43*, 6920–6937.
- [7] A. N. Banerjee, *Nanotechnol. Sci. Appl.* **2011**, *4*, 35–65.
- [8] a) M. Watanabe, *Sci. Technol. Adv. Mater.* **2017**, *18*, 705–723; b) G. Li, Z. Lian, X. Li, Y. Xu, W. Wang, D. Zhang, F. Tian, H. Li, *J. Mater. Chem. A* **2015**, *3*, 3748–3756.
- [9] a) J. Zhang, Z. Yu, Z. Gao, H. Ge, S. Zhao, C. Chen, S. Chen, X. Tong, M. Wang, Z. Zheng, Y. Qin, *Angew. Chem. Int. Ed.* **2017**, *56*, 816–820; *Angew. Chem.* **2017**, *129*, 834–838; b) C. Marchal, T. Cottineau, M. G. Méndez-Medrano, C. Colbeau-Justin, V. Caps, V. Keller, *Adv. Energy Mater.* **2018**, *8*, 1702142; c) A. Meng, J. Zhang, D. Xu, B. Cheng, J. Yu, *Appl. Catal. B* **2016**, *198*, 286–294; d) Q. Guo, C. Zhou, Z. Ma, Z. Ren, H. Fan, X. Yang, *Chem. Soc. Rev.* **2016**, *45*, 3701–3730.
- [10] a) R. Bibi, H. Huang, M. Kalulu, Q. Shen, L. Wei, O. Oderinde, N. Li, J. Zhou, *ACS Sustainable Chem. Eng.* **2019**, *7*, 4868–4877; b) S. Yuan, J. S. Qin, H. Q. Xu, J. Su, D. Rossi, Y. Chen, L. Zhang, C. Lollar, Q. Wang, H. L. Jiang, D. H. Son, H. Xu, Z. Huang, X. Zou, H. C. Zhou, *ACS Cent. Sci.* **2018**, *4*, 105–111; c) M. Dan-Hardi, C. Serre, T. Frot, L. Rozes, G. Maurin, C. Sanchez, G. Férey, *J. Am. Chem. Soc.* **2009**, *131*, 10857–10859; d) Y. Yan, C. Li, Y. Wu, J. Gao, Q. Zhang, *J. Mater. Chem. A* **2020**, *8*, 15245–15270; e) J. Cao, W. Ma, K. Lyu, L. Zhuang, H. Cong, H. Deng, *Chem. Sci.* **2020**, *11*, 3978–3985; f) C. Li, H. Xu, J. Gao, W. Du, L. Shangguan, X. Zhang, R.-B. Lin, H. Wu, W. Zhou, X. Liu, J. Yao, B. Chen, *J. Mater. Chem. A* **2019**, *7*, 11928–11933; g) A. Cadiou, N. Kolobov, S. Srinivasan, M. G. Goesten, H. Haspel, A. V. Poryvaev, M. Eddaoudi, M. V. Fedin, O. F. Mohammed, J. Gascon, *Angew. Chem. Int. Ed.* **2020**, *59*, 13468–13472; *Angew. Chem.* **2020**, *132*, 13570–13574; h) X. Chen, X. Peng, L. Jiang, X. Yuan, H. Yu, H. Wang, J. Zhang, Q. Xia, *Chem. Eng. J.* **2020**, *395*, 125080.
- [11] W.-H. Fang, L. Zhang, J. Zhang, *Chem. Soc. Rev.* **2018**, *47*, 404–421.
- [12] a) C. H. Hendon, D. Tiana, M. Fontecave, C. Sanchez, L. D'arras, C. Sassoie, L. Rozes, C. Mellot-Draznieks, A. Walsh, *J. Am. Chem. Soc.* **2013**, *135*, 10942–10945; b) S. Y. Han, D. L. Pan, H. Chen, X. B. Bu, Y. X. Gao, H. Gao, Y. Tian, G. S. Li, G. Wang, S. L. Cao, C. Q. Wan, G. C. Guo, *Angew. Chem. Int. Ed.* **2018**, *57*, 9864–9869; *Angew. Chem.* **2018**, *130*, 10012–10017.
- [13] a) Y. Keum, B. Kim, A. Byun, J. Park, *Angew. Chem. Int. Ed.* **2020**, *59*, 21591–21596; *Angew. Chem.* **2020**, *132*, 21775–21780; b) S. Yuan, T.-F. Liu, D. Feng, J. Tian, K. Wang, J. Qin, Q. Zhang, Y.-P. Chen, M. Bosch, L. Zou, S. J. Teat, S. J. Dalgarno, H.-C. Zhou, *Chem. Sci.* **2015**, *6*, 3926–3930.
- [14] a) D. Sun, S. Jang, S.-J. Yim, L. Ye, D.-P. Kim, *Adv. Funct. Mater.* **2018**, *28*, 1707110–1707116; b) F. M. Zhang, J. L. Sheng, Z. D. Yang, X. J. Sun, H. L. Tang, M. Lu, H. Dong, F. C. Shen, J. Liu, Y. Q. Lan, *Angew. Chem. Int. Ed.* **2018**, *57*, 12106–12110; *Angew. Chem.* **2018**, *130*, 12282–12286; c) L. Garzón-Tovar, J. Pérez-Carvajal, A. Yazdi, J. Hernández-Muñoz, P. Tarazona, I. Imaz, F. Zamora, D. Maspocho, *Angew. Chem. Int. Ed.* **2019**, *58*, 9512–9516; *Angew. Chem.* **2019**, *131*, 9612–9616; d) H. Peng, J. Raya, F. Richard, W. Baaziz, O. Ersen, A. Ciesielski, P. Samorì, *Angew. Chem. Int. Ed.* **2020**, *59*, 19602–19609; *Angew. Chem.* **2020**, *132*, 19770–19777.
- [15] J.-D. Xiao, L. Han, J. Luo, S.-H. Yu, H.-L. Jiang, *Angew. Chem. Int. Ed.* **2018**, *57*, 1103–1107; *Angew. Chem.* **2018**, *130*, 1115–1119.
- [16] a) M. W. Logan, S. Ayad, J. D. Adamson, T. Dilbeck, K. Hanson, F. J. Uribe-Romo, *J. Mater. Chem. A* **2017**, *5*, 11854–11863; b) Y.-F. Chen, L.-L. Tan, J.-M. Liu, S. Qin, Z.-Q. Xie, J.-F. Huang, Y.-W. Xu, L.-M. Xiao, C.-Y. Su, *Appl. Catal. B* **2017**, *206*, 426–433.
- [17] a) J. Liu, Y.-Z. Fan, X. Li, Z. Wei, Y.-W. Xu, L. Zhang, C.-Y. Su, *Appl. Catal. B* **2018**, *231*, 173–181; b) Q. Zuo, T. Liu, C. Chen, Y. Ji, X. Gong, Y. Mai, Y. Zhou, *Angew. Chem. Int. Ed.* **2019**, *58*, 10198–10203; *Angew. Chem.* **2019**, *131*, 10304–10309; c) L. Zang, H. Zhao, J. Hua, W. Cao, F. Qin, J. Yao, Y. Tian, Y. Zheng, Z. Zhang, *J. Mater. Chem. C* **2016**, *4*, 9581–9587; d) O. S. Finikova, A. V. Cheprakov, S. A. Vinogradov, *J. Org. Chem.* **2005**, *70*, 9562–9572; e) X. Fang, Q. Shang, Y. Wang, L. Jiao, T.

- Yao, Y. Li, Q. Zhang, Y. Luo, H. L. Jiang, *Adv. Mater.* **2018**, *30*, 1705112–1705118 ; f) T. He, S. Chen, B. Ni, Y. Gong, Z. Wu, L. Song, L. Gu, W. Hu, X. Wang, *Angew. Chem. Int. Ed.* **2018**, *57*, 3493–3498; *Angew. Chem.* **2018**, *130*, 3551–3556.
- [18] a) S.-Y. Ding, W. Wang, *Chem. Soc. Rev.* **2013**, *42*, 548–568; b) J. L. Segura, S. Royuela, M. Mar Ramos, *Chem. Soc. Rev.* **2019**, *48*, 3903–3945; c) X. Wang, L. Chen, S. Y. Chong, M. A. Little, Y. Wu, W. H. Zhu, R. Clowes, Y. Yan, M. A. Zwiijnenburg, R. S. Sprick, A. I. Cooper, *Nat. Chem.* **2018**, *10*, 1180–1189; d) J. Yang, A. Acharjya, M.-Y. Ye, J. Rabeah, S. Li, Z. Kochovski, S. Youk, J. Roeser, J. Grüneberg, M. Schwarze, T. Wang, Y. Lu, R. van de Krol, M. Oschatz, R. Schomäcker, P. Saalfrank, A. Thomas, C. Penschke, *Angew. Chem. Int. Ed.* **2021**, *60*, 19797–19803; *Angew. Chem.* **2021**, *133*, 19950–19956; e) W. Li, X. Huang, T. Zeng, Y. A. Liu, W. Hu, H. Yang, Y. B. Zhang, K. Wen, *Angew. Chem. Int. Ed.* **2021**, *60*, 1869–1874; *Angew. Chem.* **2021**, *133*, 1897–1902; f) R. Chen, Y. Wang, Y. Ma, A. Mal, X. Y. Gao, L. Gao, L. Qiao, X. B. Li, L. Z. Wu, C. Wang, *Nat. Commun.* **2021**, *12*, 1354; g) C. Lin, X. Liu, B. Yu, C. Han, L. Gong, C. Wang, Y. Gao, Y. Bian, J. Jiang, *ACS Appl. Mater. Interfaces* **2021**, <https://doi.org/10.1021/acsami.1021c04880>; h) J. Thote, H. B. Aiyappa, A. Deshpande, D. Díaz Díaz, S. Kurungot, R. Banerjee, *Chem. Eur. J.* **2014**, *20*, 15961–15965; i) H. Wang, C. Qian, J. Liu, Y. Zeng, D. Wang, W. Zhou, L. Gu, H. Wu, G. Liu, Y. Zhao, *J. Am. Chem. Soc.* **2020**, *142*, 4862–4871; j) S. Kandambeth, A. Mallick, B. Lukose, M. V. Mane, T. Heine, R. Banerjee, *J. Am. Chem. Soc.* **2012**, *134*, 19524–19527.
- [19] Y. Sun, L. Sun, D. Feng, H. C. Zhou, *Angew. Chem. Int. Ed.* **2016**, *55*, 6471–6475; *Angew. Chem.* **2016**, *128*, 6581–6585.
- [20] a) S. Li, H. M. Mei, S. L. Yao, Z. Y. Chen, Y. L. Lu, L. Zhang, C. Y. Su, *Chem. Sci.* **2019**, *10*, 10577–10585; b) M. Zhang, Y. Chen, J.-N. Chang, C. Jiang, W.-X. Ji, L.-Y. Li, M. Lu, L.-Z. Dong, S.-L. Li, Y.-P. Cai, Y.-Q. Lan, *JACS Au* **2021**, *1*, 212–220; c) X.-J. Kong, Z. Lin, Z.-M. Zhang, T. Zhang, W. Lin, *Angew. Chem. Int. Ed.* **2016**, *55*, 6411–6416; *Angew. Chem.* **2016**, *128*, 6521–6526; d) J. Tang, Q. Li, Y. Liu, N. Xu, K. Wang, Q. Zhang, W. Yang, Y. Fan, *Int. J. Hydrogen Energy* **2021**, *46*, 17666–17676; e) C. Lin, C. Han, H. Zhang, L. Gong, Y. Gao, H. Wang, Y. Bian, R. Li, J. Jiang, *Inorg. Chem.* **2021**, *60*, 3988–3995.
- [21] J.-D. Xiao, Q. Shang, Y. Xiong, Q. Zhang, Y. Luo, S.-H. Yu, H.-L. Jiang, *Angew. Chem. Int. Ed.* **2016**, *55*, 9389–9393; *Angew. Chem.* **2016**, *128*, 9535–9539.
- [22] M. Reza Gholipour, C.-T. Dinh, F. Béland, T.-O. Do, *Nanoscale* **2015**, *7*, 8187–8208.
- [23] G. B. Kauffman, *Chem. Educ.* **2000**, *5*, 49–53.

Manuscript received: October 17, 2021

Revised manuscript received: November 12, 2021

Accepted manuscript online: November 15, 2021

Version of record online: December 9, 2021